SIGNAL 2020

The Fifth International Conference on Advances in Signal, Image and Video Processing

ISBN: 978-1-61208-791-7

September 27th – October 1st, 2020

SIGNAL 2020 Editors

Constantin Paleologu, Polytechnic University of Bucharest, Romania

SIGNAL 2020

Forward

The Fifth International Conference on Advances in Signal, Image and Video Processing (SIGNAL 2020) continued a series of events considering the challenges in the areas of signal, image and video processing. Signal, video and image processing constitutes the basis of communications systems. With the proliferation of portable/implantable devices, embedded signal processing became widely used, despite that most of the common users are not aware of this issue. New signal, image and video processing algorithms and methods, in the context of a growing-wide range of domains (communications, medicine, finance, education, etc.) have been proposed, developed and deployed. Moreover, since the implementation platforms experience an exponential growth in terms of their performance, many signal processing techniques are reconsidered and adapted in the framework of new applications.

We take here the opportunity to warmly thank all the members of the SIGNAL 2020 technical program committee, as well as all the reviewers. The creation of such a high quality conference program would not have been possible without their involvement. We also kindly thank all the authors who dedicated much of their time and effort to contribute to SIGNAL 2020. We truly believe that, thanks to all these efforts, the final conference program consisted of top quality contributions. We also thank the members of the SIGNAL 2020 organizing committee for their help in handling the logistics of this event.

SIGNAL 2020 Chairs

SIGNAL 2020 Steering Committee
Constantin Paleologu, Polytechnic University of Bucharest, Romania
Pavel Loskot, Swansea University, UK
Wilfried Uhring, Université de Strasbourg, France
Sergey Y. Yurish, Excelera, S. L. | IFSA, Spain
Jérôme Gilles, San Diego State University, USA

SIGNAL 2020 Publicity Chair
Joseyda Jaqueline More, Universitat Politecnica de Valencia, Spain
Marta Botella-Campos, Universitat Politecnica de Valencia, Spain

SIGNAL 2020 Industry/Research Advisory Committee
Filippo Vella, National Research Council of Italy, Italy
Tudor-Catalin Zorila, Toshiba Cambridge Research Laboratory, UK
Laurent Fesquet, Grenoble Institute of Technology - TIMA, France
Zhongyuan Zhao, Beijing University of Posts and Telecommunications, China
Demetrios Sampson, Curtin University, Australia
Andrea Kutics, International Christian University, Japan

SIGNAL 2020
Committee

SIGNAL 2020 Steering Committee
Constantin Paleologu, Polytechnic University of Bucharest, Romania
Pavel Loskot, Swansea University, UK
Wilfried Uhring, Université de Strasbourg, France
Sergey Y. Yurish, Excelera, S. L. | IFSA, Spain
Jérôme Gilles, San Diego State University, USA

SIGNAL 2020 Publicity Chair
Joseyda Jaqueline More, Universitat Politecnica de Valencia, Spain
Marta Botella-Campos, Universitat Politecnica de Valencia, Spain

SIGNAL 2020 Industry/Research Advisory Committee
Filippo Vella, National Research Council of Italy, Italy
Tudor-Catalin Zorila, Toshiba Cambridge Research Laboratory, UK
Laurent Fesquet, Grenoble Institute of Technology - TIMA, France
Zhongyuan Zhao, Beijing University of Posts and Telecommunications, China
Demetrios Sampson, Curtin University, Australia
Andrea Kutics, International Christian University, Japan

SIGNAL 2020 Technical Program Committee
Waleed H. Abdulla, The University of Auckland, New Zealand
Ahmed Al Hilli, Technical College of Najaf | Al-furat Al-Awsat Technical University
Kiril Alexiev, Institute for Information and Communication Technologies -Bulgarian Academy of Sciences, Bulgaria
Djamila Aouada, SnT | University of Luxembourg, Luxembourg
Nadia Baaziz, Université du Québec en Outaouais, Canada
Junaid Baber,University of Balochistan, Pakistan
Vesh Raj Sharma Banjade, Intel Coporation, USA
Joan Bas, CTTC, Spain
Wassim Ben Chikha, Tunisia Polytechnic School, Tunisia
Stefano Berretti, University of Florence, Italy
Larbi Boubchir, LIASD - University of Paris 8, France
Moez Bouchouicha, LIS - Laboratoire d'Informatique et Systèmes | Toulon University, France
Samia Boukir, Bordeaux INP (Polytechnic Institute of Bordeaux), France
Salah Bourennane, Ecole Centrale de Marseille, France
Paula María Castro Castro, University of A Coruña, Spain
M. Girish Chandra, TCS Research & Innovation, India
Doru Florin Chiper, Technical University Gheorghe Asachi of Iasi, Romania
Silviu Ciochina, University Politehnica of Bucharest, Romania
João Dallyson Sousa de Almeida, Federal University of Maranhão, São Luís, Brazil
António Dourado, University of Coimbra, Portugal
Konstantinos Drossos, Tampere University, Finland
Laurent Fesquet, TIMA / Grenoble Institute of Technology, France
Sid Ahmed Fezza, National Institute of Telecommunications and ICT, Oran, Algeria

Table of Contents

Automatic Mesh Size Estimation in DVC for Images of Isotropic Materials

Zaira Manigrasso*, Jan Aelterman*, and Wilfried Philips*
*Department Telecommunications and Information Processing
Ghent University, Ghent 900, Belgium
Emails: {Zaira.Manigrasso, Jan.Aelterman, Wilfried.Philips}@UGent.be

***Abstract*—When non-rigid Digital Image Correlation or Digital Volume Correlation (DIC/DVC) is performed, it is critical to correctly set the parameter that determines the control point spacing for the grid on which deformation is defined. In this paper, we present a method to automatically estimate the best performing grid spacing parameter for DIC/DVC registration. The operating principle is that the optimal grid spacing parameter is a function of the image content; it may be estimated through determining the dominant feature/object size. In order to extract the information about the objects size, first, the image volume has been segmented, then the disconnected objects inside the image have been detected (using a labeling technique) and, lastly, a classification of the objects has been made based on the number of the voxels of each object. The reason for this study arises from the practical necessity of finding the best performing parameter for registration in materials sciences research. We show how an erroneous setting of the density of the control points leads to inaccurate registration. Furthermore, we demonstrate how the parameter predicted by our algorithm is indeed optimal, both in a quantitative sense, using Normalized Cross Correlation (NCC) as a measure, as well as qualitatively.**

Keywords–DIC/DVC; B-spline transformation; Grid size estimation.

I. INTRODUCTION

Digital Image Correlation (DIC) and Digital Volume Correlation (DVC) are measurement techniques that make it possible to track 2D and 3D deformations in images. These methods are typically used to obtain the full deformation and strain field [1]. In this paper, we use a DVC global approach, based on B-splines, to estimate non rigid deformations between micro Computer Tomography (micro-CT) 3D images. The deformation is calculated on a regular grid of control points defined by the spacing between the grid nodes. An incorrect choice of grid size negatively impacts not only the final deformation and strain computation [2], but also the computational time, which is linearly related to the number of the grid control points [3].

The displacement between images is characterized by global and local deformation. The global deformation is the perceived direction of the dynamic of the objects. Such direction is the result of a combination of many individual local deformations, and, in the case of non rigid motion, the local deformations have different magnitudes and directions [3][4]. With a coarse grid (large space between the grid nodes), it is only possible to describe global and smooth deformations, however, with a fine grid spacing, it is also possible to describe local and less smooth deformations [3][5]. The use of a coarse grid size is beneficial as it allows to avoid converging to overly non-smooth (and usually incorrect) solutions. By using a finer grid size, the potential to converge to a local optimum increases. The choice of the grid size is usually user dependent, however, self adapting methods have been proposed in order to reduce the dependency of the results on the user's input and in order to improve the deformation and strain accuracy [3][6][7]. These works introduce iterative methods for mesh refining. In [6], the iterative refinement is based on the concept of residual error, instead, in [3] the authors introduce a multi-level approach. For each level, they introduce a control point status associated with each control point, marking it either active or passive. The state is associated with the value of a similarity metric. In [7], the self-adapting algorithm affects the order of the elements of the grid and not their dimensions.

TABLE I. THE BEST PERFORMING GRID SIZE FOR EACH DATASET WITH THE RELATIVE NCC VALUE RESULTED FROM DVC

	Aluminum foam	Leavening dough	Lede stone
Optimal grid size [voxels]	37	22	40
NCC	0.992	0.995	0.991

In this paper, we investigate the idea that, for isotropic materials, the optimal grid size is a function of the image content in a way that the motion of small objects inside the images is better tracked using a fine grid and, vice versa, a coarse mesh can better define the motion of larger objects. Since the B-spline transformation is based on a uniform grid of control points, we tried to link the distance between control points with the most dominant material structure dimension. Our hypothesis is that the most frequently occurring material structure dimension is a good predictor for the optimal grid size in the non rigid DIC/DVC approach. In our study, we applied DVC on six different datasets using a range of different grid size parameters. What has emerged is not only that the estimated deformation field significantly depends on the size parameter, but also that the same grid size is not suitable for all the datasets (Table I).

The rest of the paper is structured as follows. Section II aims to describe the workflow to obtain the optimal grid size spacing for non rigid DIC/DVC. In the Sections III and IV, the details of the DVC experiment and the datasets used are covered, respectively. Results, discussions and conclusion are given in Sections V and VI.

II. PROPOSED METHOD

This method operates from the principle that the optimal grid spacing is a function of the image content. It assumes the characteristic size of the most frequently occurring material structure is indicative of the easiest tracking, as well as the resolution at which deformation can be reliably tracked, and it is, therefore, a good predictor for the optimal grid size in DIC/DVC.

The method consists of 3 steps that are summarized in Figure 1. The purpose of the first step is to segment the objects present in the images in order to measure the size of each of them (Figure 1A). Once the segmentation has been done and the histogram of the objects size

TABLE II. STONE SCANNING SETTINGS

	Lede stone
Acquisition time	48 min
Voxel size	0.02 mm
Volume dimension	1014x1014x752

TABLE III. ALUMINUM FOAM AND LEAVENING DOUGH SCANNING SETTINGS

	Aluminum foam	Leavening dough
Acquisition time	14 min	30 min
Number of gantry rotation	60	75
Number of projection per rotation	700	800
Total compression per rotation	$\pm 133\mu m$	-
Total compression	$\pm 8mm$	-
Voxel size	0.02 mm	0.02 mm
Volume dimension	512x512x512	640x640x640

distribution has been created (Figure 1B), the grid size for the image registration is set (Figure 1C). A detailed explanation of each of the 3 steps is provided in the following subsections.

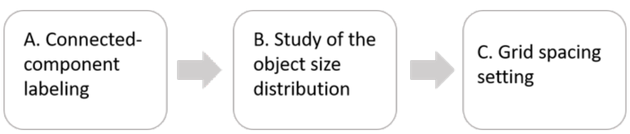

Figure 1. Flowchart of the method.

A. *Connected-component labeling*

Through labeling techniques, we start by distinguishing different disconnected parts of a phase in the image. In micro-CT, these parts represent characteristic small "objects" (e.g., pores, bubbles, nodules). The input of the labeling algorithm is the segmented dataset (binary image), where the voxels belonging to the objects which we want to label are part of the foreground voxels (label = 1) and all other voxels are part of the background (label = 0). The labeling detects each component of foreground voxels and assigns a unique label to all voxels of each object. The labeling algorithm used [8] is based on iterative recursion. The algorithm starts from (0,0,0) voxels and finds the first unlabelled voxel (label = 1) v_1. A cuboid sub-volume is created starting from v_1 and all the voxels inside the volume with label 1 are changed into the label l if they are 26-connected to v_1. For the border voxels of the sub-volume, the procedure done to v_1 is repeated until all the voxels 26-connected to v_1 are marked with l. At the end of the first iteration, the value of the label, l, is incremented by 1 and the algorithm finds the next unlabelled object voxel v_2 and repeats the same procedure done to v_1. The resulted objects are color labeled (different colors for different objects). For each object, its size (in number of voxel) is calculated. Lastly, a histogram that summarizes the number of objects of each size is created.

B. *Study of the object size distribution*

Once the histogram has been created, the dominant object size is taken as a good predictor of the grid spacing: the region

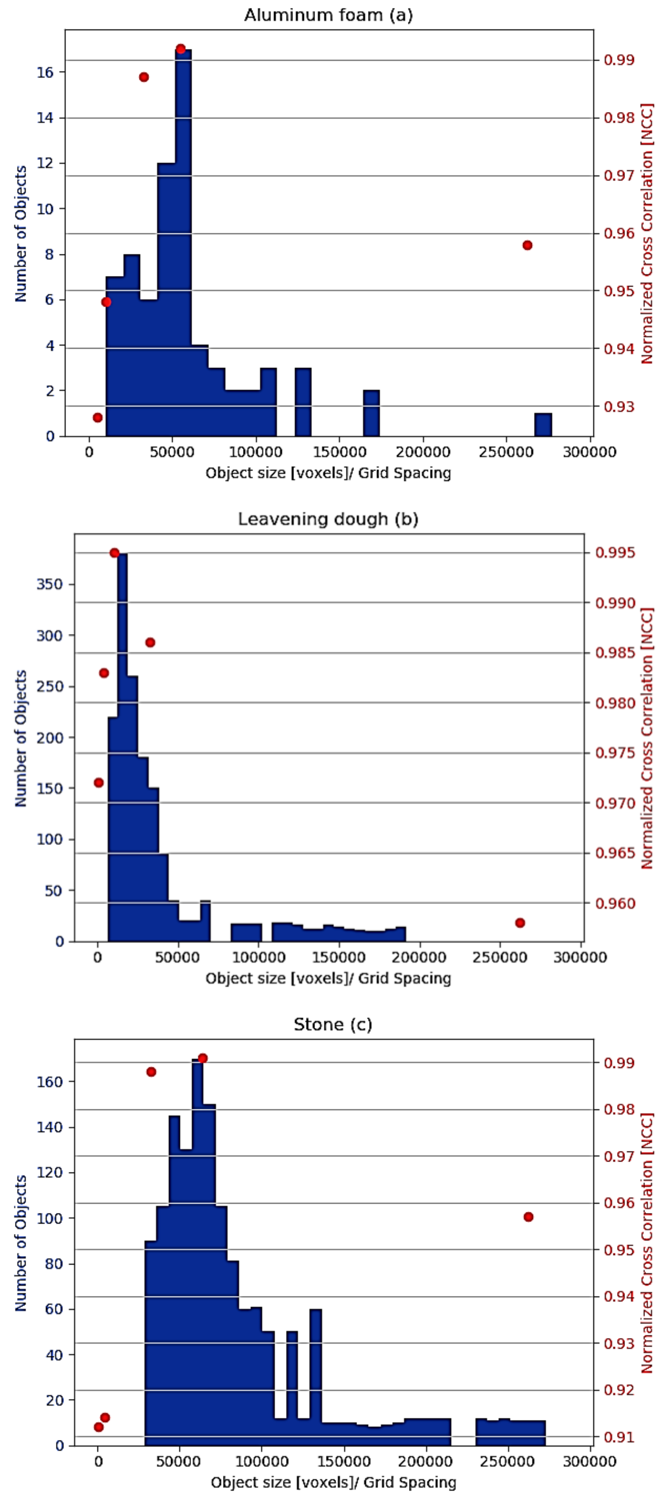

Figure 2. Plot of the registration performance expressed using NCC metric as function of the grid size spacing. On the same graph, the distribution of the objects size inside the image is shown.

around the peak of the histogram is the predicted value for the grid spacing.

C. Grid spacing setting

Since in each dataset there are different structures/objects with different dimensions, it is not possible to match all the structures with an uniform grid, typical of B-spline based DVC. The cells of the grid can be both cubic or rectangular cuboid. For this experiment, cubic cells have been used with the edge length given by the cubic root of the most occurring object size (most numerous class) in voxels.

III. Experimental setup

The experiment has the dual purpose of investigating the influence of the different grid size settings on the deformation estimate and of testing our hypothesis, which is that the optimal grid size setting is related to the most frequently occurring material structure size. The experiment evaluates four different grid sizes, with the length of the edge of the cubic cell given by the powers of 2 (2^3, 2^4, 2^5, 2^6). The registration has also been performed with a cubic cell grid with the edge length equal to the cubic root of the most occurring object dimension inside the dataset. For each registration, the NCC value was calculated in order to compare the results quantitatively.

The chosen transformation is the B-spline. Among the splines functions (e.g., Hermite, plate), B-splines is a popular choice because of its properties of locality, continuity and affine-invariance [9][10]. Because the CT attenuation images are based on the constancy of brightness, NCC is a suitable registration cost function. For minimising it, Adaptative Stochastic Gradient Descent (ASGD) was used [11].

IV. Experimental data

Six different micro-CT 3D datasets were used in this experiment. Three of them are from different materials, exhibiting different dynamics: compression of aluminum foam (Table III), leavening of bread dough (Table III) and water absorption of stone (Lede type) (Table II). To evaluate our claims further, three additional datasets have been created artificially, decreasing the resolution of the previous dataset by a factor of 2 in the 3 dimensions.

The aluminum foam and the leavening dough dataset have been acquired using the Environmental Micro-CT (EMCT) scanner of the Ghent University Centre of X-ray Tomography (UGCT). The Lede stone has been acquired using Tescan CoreTOM. The first two datasets have been acquired during the deformation processes (dynamic scan), whereas the last dataset has been acquired before and after the deformation process (static scan).

V. Results

From the classified data and from their representation by using the histogram, the most dominant object size for each dataset has been extracted. In the case of aluminum foam, the most numerous class, indicating the dimension of the objects inside the image volume, corresponds to 37^3 voxels. To this class belong 18 out of 76 objects (23.68%). Setting the cubic grid size for DVC with the edge length of 37 pixels, the NCC value reaches the peak of 0.992. It is clearly visible

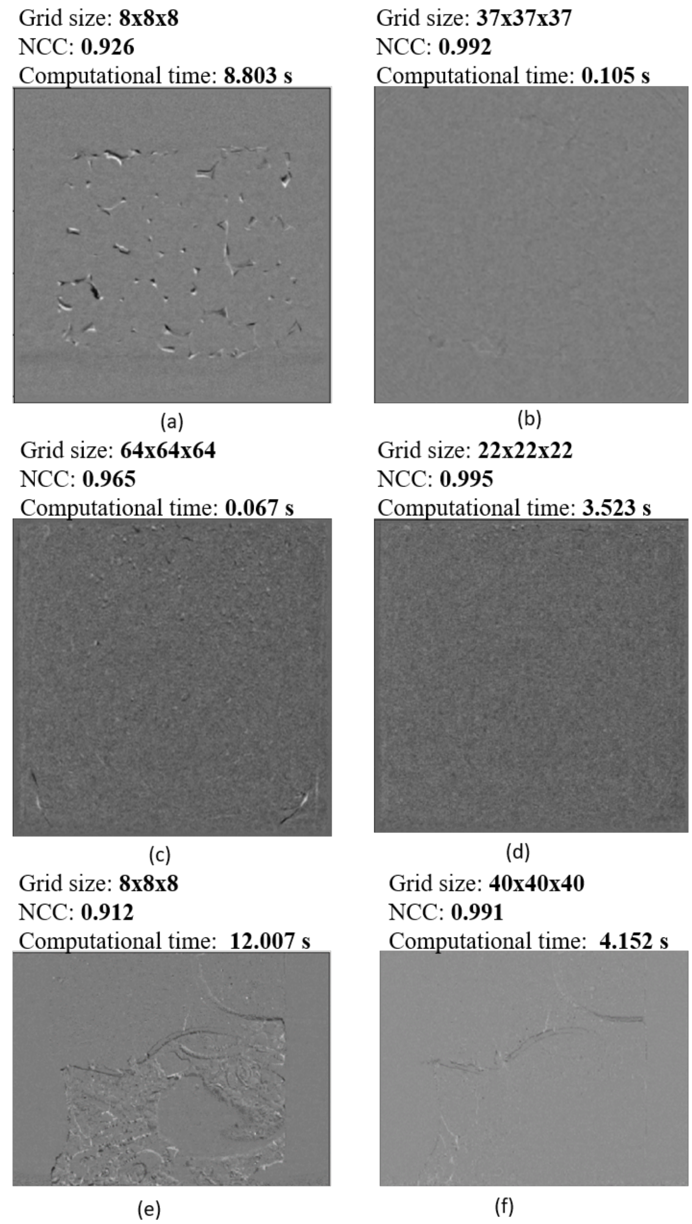

Figure 3. Results of DVC with different grid size settings. (a)-(b): z-y slice of the difference between transformed and reference image of the aluminum foam at full resolution (512x512x512); (c)-(d): z-y slice of the difference between transformed and reference image of the leavening dough at full resolution (640x640x640); (d)-(e): z-y slice of the difference between transformed and reference image of the Lede stone at full resolution (1014x1014x752). The computational time is meant for one DVC iteration.

in Figure 2: the peak of the metric value coincides with the peak of the classified data. From the histogram, it is visible a range going from $16^3 - 40^3$ where most of the objects belong. The NCC value in this interval is high and decreases significantly for those grid size values for which the number of objects inside the image with the same dimension is low or even null. For the aluminum foam, the worst NCC value corresponds to 8^3 (Figures 2 and 3(a)). In Figure 3, there is a qualitative comparison between the registration with different grid sizes. The most numerous class indicating the dimension of the objects for leavening dough and Lede stone are 22^3 and 40^3, respectively. For the leavening dough, most of the objects (73.33%) belong to the interval $15^3 - 30^3$. At the extremes of the range, NCC reaches the vales of 0.983 and 0.985, with a peak of 0.995 in correspondence of the peak of the histogram. For the Lede stone, the most likely interval is $24^3 - 48^3$ with 73.33% , with NCC values at the extremes of the interval of 0.989 and 0.954 and a peak of 0.991 corresponding to the value of grid size of 40^3. As in the case of the aluminum foam, the NCC value decreases considerably if there are no objects which match the grid size. In the case of the leavening dough, the worst registration result has been obtained with the grid cell dimension of 64^3 (NCC = 0.965) (Figure 3(c)), followed by the result obtained with the grid size of 8^3 (NCC = 0.975) (Figure 2). The Lede stone dataset has low NCC value for grid sizes of 8^3 (NCC=0.912) and 16^3 (NCC=0.913) (Figure 2 and 3).

To have more evidence about the validity of the proposed method, the same experiment has been repeated on the same datasets at lower resolution. The resolution has been decreased by a factor of 2 along the three dimensions. According to our hypothesis, the optimal value of the grid size should be different from the previous value on the full resolution dataset. Since the resolution has been decreased by a factor of 2, the dimensions of the objects/structures inside the image are also smaller and, therefore, the optimal distances between the nodes of the grid are reduced by a factor of 2. The results of the experiment are reported in Figure 4.

VI. Conclusion

The study carried out in this paper confirms our initial hypothesis: the best performing value for the grid spacing parameter is linked to the most occurring material structure size. The advantage of this method compared with other techniques present in literature [3][6][7] is that it is able to give to the user prior information about the optimal grid size ready to be used in many of the open source libraries and commercial software for DVC.

With this research, we are not suggesting that this parameter optimization method is globally optimal, instead, we suggest that it may be a practically useful heuristic to automate DVC/DIC algorithms. Indeed, in a purely theoretical sense, the optimal grid size decision should additionally depend on the kinematics of the material sample, not just its structural makeup. In this study, the nature of the deformation is not taken in consideration, as it could be argued that it is unrealistic anyhow to expect software to track motion fields that are erratic on a finer resolution scale than the finest resolution of the visible structures.

With this study, we are able to give some guidelines for the setting of the optimal grid spacing parameter for DVC/DIC in order to be less user dependent. Furthermore, being an automated method, it is possible to integrate it in a future software for DVC.

Acknowledgment

This work was funded by the Research Foundation — Flanders in the Strategic Basic Research Programme (FWO-SBO), file number S003418N. The authors thank UGCT (UGent, Centre for X-ray Tomography) for the aluminum foam and leavening dough dataset, Dr. Tim De Kock (FWO post doctoral research fellow at the time of the acquisition) and TESCAN-XRE for the dataset of Lede stone.

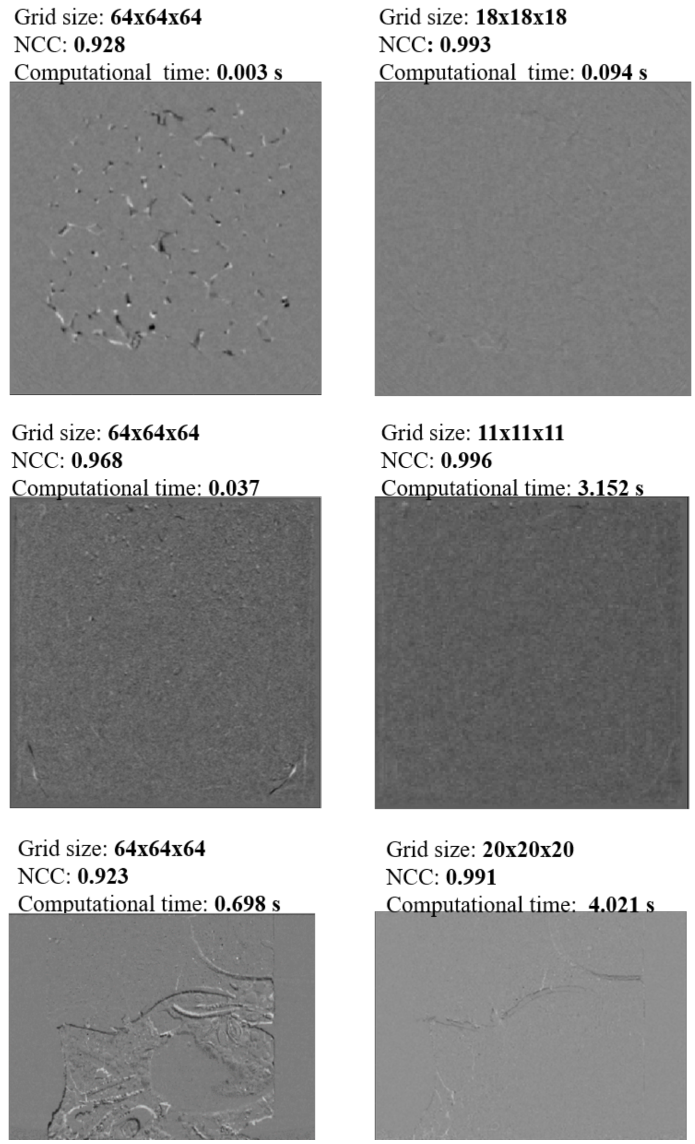

Figure 4. Results of DVC with different grid size settings. (a)-(b): z-y slice of the difference between transformed and reference image of the aluminum foam at half resolution (256x256x256); (c)-(d): z-y slice of the difference between transformed and reference image of the leavening dough at half resolution (320x320x320); (d)-(e): z-y slice of the difference between transformed and reference image of the Lede stone at half resolution (507x507x376).The computational time is meant for one DVC iteration.

References

[1] B. Bay, T. Smith, D. Fyhrie, and M. Saad, “Digital Volume Correlation: Three-dimensional Strain Mapping Using X-ray Tomography ,” Experimental Mechanics, vol. 39, 1999, pp. 217–226.

[2] F. Mortazavi, “Development of a global digital image correlation approach for a fast high-resolution displacement measurements,” PhD thesis, École Polytechnique de Montréal., 2013.

[3] J. Schnabel, “A generic Framework for Non-Rigid Registration Based on Non-uniform Multi-level free-Form Deformations,” Medical Image Computing and Computer-Assisted Intervention – MICCAI, 2001, pp. 573–581.

[4] S. Klein, M. Staring, K. Murphy, M. Viergever, and J. Pluim, “elastix: a toolbox for intensity based medical image registration,” IEEE Transactions on Medical Imaging, vol. 29, 2010, pp. 196–205.

[5] L. Zhang, M. Li, and F. P. Hou, W., “Registration of Lung CT Images Using B-spline Based Free-Form Deformation,” IEEE International Conference on Progress in Informatics and Computing (PIC), 2018.

[6] X. Wang and S. Ma, “Mesh-Based Digital Image Correlation Method Using Non-Uniform Elements for Measuring Displacement Fields with High Gradient,” Experimental Mechanics, vol. 54, 2014, pp. 1545 – 1554.

[7] L. Wittevrongel, S. Lava, P. Lomov, and D. Debruyne, “A Self Adaptive Global Digital Image Correlation Algorithm,” Experimental Mechanics, vol. 55, 2014, pp. 361–378.

[8] Q. Hu, G. Qian, and W. Nowinski, “Fast connected-component labelling in three-dimensional binary images based on iterative recursion,” Computer Vision and Image Understanding, vol. 99, 2005, pp. 414–434.

[9] L. Piegl and W. Tiller, The NURBS book. Springer Science Business Media, 1996.

[10] Y. Yin, E. Hoffman, and C. Lin, “Mass preserving nonrigid registration of CT lung images using cubic B-spline,” Medical Physics, vol. 36, 2009, pp. 4213–4222.

[11] S. Klein, J. Pluim, M. Staring, and M. Viergever, “Adaptive stochastic gradient descent optimisation for image registration ,” International journal of Computer Vision, vol. 81, 2009, pp. 227–239.

 ISBN: 978-1-61208-791-7

Global Stability of Positive Different Fractional Orders Nonlinear Feedback Systems

Tadeusz Kaczorek
Faculty of Electrical Engineering
Bialystok University of Technology
Bialystok, Poland
e-mail: kaczorek@ee.pw.edu.pl

Lukasz Sajewski
Faculty of Electrical Engineering
Bialystok University of Technology
Bialystok, Poland
e-mail: l.sajewski@pb.edu.pl

***Abstract*—The global stability of continuous-time fractional orders nonlinear feedback systems with positive linear parts is investigated. New sufficient conditions for the global stability of these class of positive nonlinear systems are established. The effectiveness of these new stability conditions is demonstrated on a simple example.**

Keywords-global stability; fractional order; positive; nonlinear; feedback system.

I. INTRODUCTION

In positive systems inputs, state variables and outputs take only nonnegative values for any nonnegative inputs and nonnegative initial conditions [1][4][9]. Examples of positive systems are industrial processes involving chemical reactors, heat exchangers and distillation columns, storage systems, compartmental systems, water and atmospheric pollution models, and so on. A variety of models having positive behavior can be found in engineering, management science, economics, social sciences, biology and medicine. An overview of state of the art in positive systems theory is given in the monographs [1][4][9][13][18].

Mathematical fundamentals of the fractional calculus are given in the monographs [13][18][23][24]. Positive fractional linear systems have been investigated in [3][5][7][10]-[14][17][21][24][25][26]. Positive linear systems with different fractional orders have been addressed in [10][11][28]. Descriptor positive systems have been analyzed in [2][28]. Linear positive electrical circuits with state feedback have been addressed in [2][18]. The superstabilization of positive linear electrical circuits by state feedback has been analyzed in [16] and the stability of nonlinear systems in [17][18]. The global stability of nonlinear systems with negative feedback and not necessary asymptotically stable positive linear parts has been investigated in [6][8]. The global stability of nonlinear standard and fractional positive feedback systems has been considered in [15].

In this paper, the global stability of nonlinear fractional orders feedback systems with positive linear parts will be addressed.

The paper is organized as follows. In Section 2, the basic definitions and theorems concerning the positive different fractional orders linear systems are recalled. New sufficient conditions for the global stability feedback nonlinear systems with positive linear parts are established in Section 3. Concluding remarks are given in Section 4.

The following notation will be used: $\Re$ - the set of real numbers, $\Re^{n\times m}$ - the set of $n\times m$ real matrices, $\Re_+^{n\times m}$ - the set of $n\times m$ real matrices with nonnegative entries and $\Re_+^n = \Re_+^{n\times 1}$, M_n - the set of $n\times n$ Metzler matrices (real matrices with nonnegative off-diagonal entries), I_n - the $n\times n$ identity matrix.

II. PRELIMINARIES

Consider the fractional continuous-time linear system

$$\frac{d^\alpha x(t)}{dt^\alpha} = Ax(t) + Bu(t), \tag{1a}$$

$$y(t) = Cx(t), \tag{1b}$$

where $x(t)\in\Re^n$, $u(t)\in\Re^m$, $y(t)\in\Re^p$ are the state, input and output vectors, $A\in\Re^{n\times n}$, $B\in\Re^{n\times m}$, $C\in\Re^{p\times n}$. In this paper, the following Caputo definition of the fractional derivative of α order will be used [13][18][23][24]

$${}_0D_t^\alpha f(t) = \frac{d^\alpha f(t)}{dt^\alpha} = \frac{1}{\Gamma(1-\alpha)}\int_0^t \frac{\dot f(\tau)}{(t-\tau)^\alpha}d\tau, \quad 0<\alpha<1, \tag{2}$$

where $\dot f(\tau) = \frac{df(\tau)}{d\tau}$ and $\Gamma(x) = \int_0^\infty t^{x-1}e^{-t}dt$, $\mathrm{Re}(x) > 0$ is the Euler gamma function.

Definition 1. [13][18] The fractional system (1) is called (internally) positive if $x(t)\in\Re_+^n$ and $y(t)\in\Re_+^p$, $t\ge 0$ for any initial conditions $x(0)\in\Re_+^n$ and all inputs $u(t)\in\Re_+^m$, $t\ge 0$.

Theorem 1. [13] [18] The fractional system (1) is positive if and only if

$$A\in M_n,\ B\in\Re_+^{n\times m},\ C\in\Re_+^{p\times n}. \tag{3}$$

Definition 2. The fractional positive linear system (1) is called asymptotically stable (and the matrix A Hurwitz) if

$$\lim_{t\to\infty} x(t) = 0 \text{ for all } x(0)\in \Re_+^n . \tag{4}$$

The positive fractional system (1) is asymptotically stable if and only if the real parts of all eigenvalues s_k of the matrix A are negative, i.e. $\operatorname{Re} s_k < 0$ for $k = 1,...,n$ [13] [18].

Theorem 2. The positive fractional system (7) is asymptotically stable if and only if one of the following equivalent conditions is satisfied:

1) All coefficients of the characteristic polynomial

$$\det[I_n s - A] = s^n + a_{n-1}s^{n-1} + ... + a_1 s + a_0 \tag{5}$$

are positive, i.e. $a_i > 0$ for $i = 0,1,...,n-1$.

2) There exists strictly positive vector $\lambda = [\lambda_1 \ \cdots \ \lambda_n]$, $\lambda_k > 0$, $k = 1,...,n$ such that

$$A\lambda < 0 \text{ or } \lambda^T A < 0 . \tag{6}$$

The transfer matrix of the system (1) is given by

$$T(s^\alpha) = C[I_n s^\alpha - A]^{-1} B . \tag{7}$$

Now, consider the fractional linear system with two different fractional order

$$\begin{bmatrix} \dfrac{d^\alpha x_1(t)}{dt^\alpha} \\ \dfrac{d^\beta x_2(t)}{dt^\beta} \end{bmatrix} = \begin{bmatrix} A_{11} & A_{12} \\ A_{21} & A_{22} \end{bmatrix}\begin{bmatrix} x_1(t) \\ x_2(t) \end{bmatrix} + \begin{bmatrix} B_1 \\ B_2 \end{bmatrix} u(t) , \tag{8a}$$

$$y(t) = [C_1 \quad C_2]\begin{bmatrix} x_1(t) \\ x_2(t) \end{bmatrix}, \tag{8b}$$

where $0 < \alpha, \beta < 1$, $x_1(t) \in \Re^{n_1}$ and $x_2(t) \in \Re^{n_2}$ are the state vectors, $A_{ij} \in \Re^{n_i \times n_j}$, $B_i \in \Re^{n_i \times m}$, $C_i \in \Re^{p \times n_i}$; i, j = 1,2; $u(t) \in \Re^m$ is the input vector and $y(t) \in \Re^p$ is the output vector. Initial conditions for (8) have the form

$$x_1(0) = x_{10} , \ x_2(0) = x_{20} \text{ and } x_0 = \begin{bmatrix} x_{10} \\ x_{20} \end{bmatrix} . \tag{9}$$

Remark 1. The state equation (8) of fractional continuous-time linear systems with two different fractional orders has a similar structure as the 2D Roeesser type models.

Definition 3. The fractional system (8) is called positive if $x_1(t) \in \Re_+^{n_1}$ and $x_2(t) \in \Re_+^{n_2}$, $t \ge 0$ for any initial conditions $x_{10} \in \Re_+^{n_1}$, $x_{20} \in \Re_+^{n_2}$ and all input vectors $u \in \Re_+^m$, $t \ge 0$.

Theorem 3. The fractional system (8) for $0 < \alpha < 1;\ 0 < \beta < 1$ is positive if and only if

$$\overline{A} = \begin{bmatrix} A_{11} & A_{12} \\ A_{21} & A_{22} \end{bmatrix} \in M_N , \ \overline{B} = \begin{bmatrix} B_1 \\ B_2 \end{bmatrix} \in \Re_+^{N\times m} ,$$

$$C = [C_1 \quad C_2] \in \Re_+^{p\times n} \ (N = n_1 + n_2) . \tag{10}$$

Theorem 4. The positive fractional system (8) is asymptotically stable if and only if one of the following equivalent conditions is satisfied:

1) All coefficients of the characteristic polynomial

$$\det[I_n s - \overline{A}] = s^n + \overline{a}_{n-1}s^{n-1} + ... + \overline{a}_1 s + \overline{a}_0 \tag{11}$$

are positive, i.e. $\overline{a}_i > 0$ for $i = 0,1,...,n-1$.

2) There exists strictly positive vector $\lambda = [\lambda_1 \ \cdots \ \lambda_n]$, $\lambda_k > 0$, $k = 1,...,n$ such that

$$\overline{A}\lambda < 0 \text{ or } \lambda^T \overline{A} < 0 . \tag{12}$$

Theorem 5. The solution of the equation (8a) for $0 < \alpha < 1;\ 0 < \beta < 1$ with initial conditions (9) has the form

$$x(t) = \begin{bmatrix} x_1(t) \\ x_2(t) \end{bmatrix} = \Phi_0(t)x_0 + \int_0^t M(t-\tau)u(\tau)d\tau , \tag{13}$$

where

$$\begin{aligned} M(t) &= \Phi_1(t)B_{10} + \Phi_2(t)B_{01} \\ &= \begin{bmatrix} \Phi_{11}^1(t) & \Phi_{12}^1(t) \\ \Phi_{21}^1(t) & \Phi_{22}^1(t) \end{bmatrix}\begin{bmatrix} B_1 \\ 0 \end{bmatrix} + \begin{bmatrix} \Phi_{11}^2(t) & \Phi_{12}^2(t) \\ \Phi_{21}^2(t) & \Phi_{22}^2(t) \end{bmatrix}\begin{bmatrix} 0 \\ B_2 \end{bmatrix} \\ &= \begin{bmatrix} \Phi_{11}^1(t)B_1 + \Phi_{12}^2(t)B_2 \\ \Phi_{21}^1(t)B_1 + \Phi_{22}^2(t)B_2 \end{bmatrix} = \begin{bmatrix} \Phi_{11}^1(t) & \Phi_{12}^2(t) \\ \Phi_{21}^1(t) & \Phi_{22}^2(t) \end{bmatrix}\begin{bmatrix} B_1 \\ B_2 \end{bmatrix} \end{aligned} \tag{14a}$$

and

$$\Phi_0(t) = \sum_{k=0}^{\infty}\sum_{l=0}^{\infty} T_{kl} \frac{t^{k\alpha + l\beta}}{\Gamma(k\alpha + l\beta + 1)} , \tag{14b}$$

$$\Phi_1(t) = \sum_{k=0}^{\infty}\sum_{l=0}^{\infty} T_{kl} \frac{t^{(k+1)\alpha + l\beta - 1}}{\Gamma[(k+1)\alpha + l\beta]} , \tag{14c}$$

$$\Phi_2(t)=\sum_{k=0}^{\infty}\sum_{l=0}^{\infty}T_{kl}\frac{t^{k\alpha+(l+1)\beta-1}}{\Gamma[k\alpha+(l+1)\beta]}, \tag{14d}$$

$$T_{kl}=\begin{cases} I_n & \text{for } k=l=0 \\ \begin{bmatrix} A_{11} & A_{12} \\ 0 & 0 \end{bmatrix} & \text{for } k=1, l=0 \\ \begin{bmatrix} 0 & 0 \\ A_{21} & A_{22} \end{bmatrix} & \text{for } k=0, l=1 \\ T_{10}T_{k-1,l}+T_{01}T_{k,l-1} & \text{for } k+l>1 \end{cases} \tag{14e}$$

The proof is given in [11].
Note that, if $\alpha=\beta$, then from (13) we have

$$\Phi_0\big|_{\alpha=\beta}(t)=\sum_{k=0}^{\infty}\frac{A^k t^{k\alpha}}{\Gamma(k\alpha+1)}. \tag{15}$$

The transfer matrix of the system (8) is given by

$$T(s^\alpha, s^\beta)=\overline{C}\left[\begin{bmatrix} I_{n_1}s^\alpha & 0 \\ 0 & I_{n_2}s^\beta \end{bmatrix}-\overline{A}\right]^{-1}\overline{B}. \tag{16}$$

III. FRACTIONAL DIFFERENT ORDERS NONLINEAR FEEDBACK SYSTEMS WITH POSITIVE LINEAR PARTS

Consider the nonlinear feedback system shown in Figure 1, which consists of the positive linear part, the nonlinear element with characteristic $u=f(e)$ and the positive scalar feedback. The positive linear part is described by the equations

$$\begin{bmatrix} \frac{d^\alpha x_1(t)}{dt^\alpha} \\ \frac{d^\beta x_2(t)}{dt^\beta} \end{bmatrix}=\overline{A}\begin{bmatrix} x_1(t) \\ x_2(t) \end{bmatrix}+\overline{B}u(t),$$
$$y(t)=\overline{C}\begin{bmatrix} x_1(t) \\ x_2(t) \end{bmatrix}, \tag{17}$$

where $0<\alpha,\beta<1$, $x_1=x_1(t)\in\Re^{n_1}$ and $x_2=x_2(t)\in\Re_+^{n_2}$ are the state vectors, $u=u(t)\in\Re$ is the input vector, $y=y(t)\in\Re$ is the input vector, matrices $\overline{A}$, $\overline{B}$, $\overline{C}$ for $p=m=1$ are defined by (10).

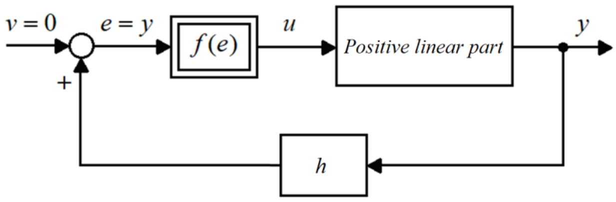

Figure 1. The nonlinear feedback system.

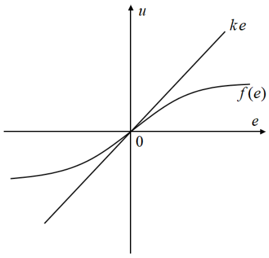

Figure 2. Characteristic of the nonlinear element.

The characteristic of the nonlinear element is shown in Figure 2 and it satisfies the condition

$$0<f(e)<ke,\ \ 0<k<\infty. \tag{18}$$

It is assumed that the positive linear part is asymptotically stable (the matrix $\overline{A}\in M_n$ is Hurwitz).

Definition 4. The nonlinear positive system is called globally stable if it is asymptotically stable for all nonnegative initial conditions $\begin{bmatrix} x_{10} \\ x_{20} \end{bmatrix}\in\Re_+^n$.

The following theorem gives sufficient conditions for the global stability of the positive nonlinear system.

Theorem 6. The nonlinear system consisting of the positive linear part, the nonlinear element satisfying the condition (18) and the positive scalar feedback *h* is globally stable if the matrix

$$\overline{A}+kh\overline{B}\overline{C}\in M_n \tag{19}$$

is asymptotically stable (Hurwitz matrix).

Matrices $\overline{A}$, $\overline{B}$, $\overline{C}$ are given by (10).

Proof. The proof will be accomplished by the use of the Lyapunov method [19][20]. As the Lyapunov function $\overline{V}(x)$, we choose

$$\overline{V}(x)=V_1(x)+V_2(x)=\lambda_1^T x_1+\lambda_2^T x_2\geq 0 \text{ for}$$
$$\overline{x}=\begin{bmatrix} x_1 \\ x_2 \end{bmatrix}\in\Re_+^n,\ \ \overline{\lambda}=\begin{bmatrix} \lambda_1 \\ \lambda_2 \end{bmatrix}\in\Re_+^n, \tag{20}$$

where $\overline{\lambda}$ are strictly positive vectors with all positive components.
Using (20) and (17), we obtain

$$\frac{d^\alpha V_1(x)}{dt^\alpha}+\frac{d^\beta V_2(x)}{dt^\beta}=[\lambda_1^T \quad \lambda_2^T]\begin{bmatrix}\frac{d^\alpha x_1}{dt^\alpha}\\ \frac{d^\beta x_2}{dt^\beta}\end{bmatrix} \tag{21}$$
$$=\overline{\lambda}^T(\overline{A}\overline{x}+\overline{B}u)\le\overline{\lambda}^T(\overline{A}x+kh\overline{B}\overline{C})\overline{x}$$

since $u=f(e)\le ke=kh\overline{C}\overline{x}$.

From (21), it follows that $\frac{d^\alpha V_1(x)}{dt^\alpha}+\frac{d^\beta V_2(x)}{dt^\beta}<0$ if the matrix (19) is Hurwitz and the nonlinear system is globally stable. □

Example 1. Consider the nonlinear system with the positive linear part with the matrices

$$A=\begin{bmatrix}-3 & 0.5 & 0.2 & 0.1\\ 1 & -2 & 0.2 & 0.3\\ 0.2 & 0.3 & -5 & 0.4\\ 0.3 & 0.4 & 0.5 & -4\end{bmatrix},\ B=\begin{bmatrix}0.5\\0.2\\0.6\\0.4\end{bmatrix},\ C=[0.2 \quad 0.4 \quad 0.5 \quad 0.3],$$
$$h=0.5,\ \alpha=0.4,\ \beta=0.6,\ n_1=n_2=2, \tag{22}$$

the nonlinear element satisfying the condition (18) and the positive feedback with gain *h*. Find *k* satisfying (19) for which the nonlinear system is globally stable for $h=0.5$.
Using (14) and (17) for $h=0.5$, we obtain

$$\hat{A}=\overline{A}+kh\overline{B}\overline{C}=\begin{bmatrix}A_{11} & A_{12}\\ A_{21} & A_{22}\end{bmatrix}+kh\begin{bmatrix}B_1\\B_2\end{bmatrix}[C_1 \quad C_2]$$
$$=\begin{bmatrix}-3+0.05k & 0.5+0.1k & 0.2+0.125k & 0.1+0.075k\\ 1+0.02k & -2+0.04k & 0.2+0.05k & 0.3+0.03k\\ 0.2+0.06k & 0.3+0.12k & -5+0.15k & 0.4+0.09k\\ 0.3+0.04k & 0.4+0.08k & 0.5+0.1k & -4+0.06k\end{bmatrix}. \tag{23}$$

The characteristic polynomial of the matrix (23) has the form

$$\det(I_4s-\hat{A})=s^4+(14-0.3k)s^3+(70.05-3.31k)s^2$$
$$+(146.39-11.99k)s+(104.64-14.28k) \tag{24}$$

and its coefficients are positive, which implies that the nonlinear system with (22) is globally stable for $k<7.33$.

Remark 1. The determinant of the matrix (23) has the form

$$\det(\hat{A})=104.64-14.28k \tag{25}$$

and it is equal to zero for $k=7.33$.

IV. CONCLUSIONS

The global stability of continuous-time different fractional orders nonlinear feedback systems with positive linear parts and positive scalar feedback has been investigated. New sufficient conditions for the global stability of this class of positive nonlinear systems have been established (Theorem 6). The effectiveness of these new stability conditions has been demonstrated on simple a example of positive nonlinear different orders system. The considerations can be extended to discrete-time standard fractional different orders nonlinear systems with positive linear parts and scalar feedback. An open problem is an extension of the considerations to nonlinear different orders fractional systems with interval matrices of their positive linear parts.

ACKNOWLEDGMENT

This work was supported by National Science Centre in Poland under work No. 2017/27/B/ST7/02443.

REFERENCES

[1] A. Berman and R. J. Plemmons, Nonnegative Matrices in the Mathematical Sciences, SIAM, 1994.

[2] K. Borawski, “Modification of the stability and positivity of standard and descriptor linear electrical circuits by state feedbacks”, Electrical Review, vol. 93, no. 11, 2017, pp. 176-180.

[3] M. Busłowicz and T. Kaczorek, “Simple conditions for practical stability of positive fractional discrete-time linear systems”, Int. J. Appl. Math. Comput. Sci., vol. 19, no. 2, 2009, pp. 263-169.

[4] L. Farina and S. Rinaldi, Positive Linear Systems; Theory and Applications, J. Wiley, New York, 2000.

[5] T. Kaczorek, “Absolute stability of a class of fractional positive nonlinear systems”, Int. J. Appl. Math. Comput. Sci., 2019, vol. 29, no. 1, pp. 93-98.

[6] T. Kaczorek, “Analysis of positivity and stability of discrete-time and continuous-time nonlinear systems”, Computational Problems of Electrical Engineering, vol. 5, no. 1, 2015, pp. 11-16.

[7] T. Kaczorek, “Analysis of positivity and stability of fractional discrete-time nonlinear systems”, Bull. Pol. Acad. Sci. Techn., vol. 64, no. 3, 2016, pp. 491-494.

[8] T. Kaczorek, “Global stability of nonlinear feedback systems with positive linear parts”, International Journal of Nonlinear Sciences and Numerical Simulation, vol. 20, no. 5, 2019, pp. 575-579.

[9] T. Kaczorek, Positive 1D and 2D Systems, Springer-Verlag, London, 2002.

[10] T. Kaczorek, “Positive linear systems with different fractional orders”, Bull. Pol. Acad. Sci. Techn., vol. 58, no. 3, 2010, pp. 453-458.

[11] T. Kaczorek, “Positive linear systems consisting of n subsystems with different fractional orders”, IEEE Trans. on Circuits and Systems, vol. 58, no. 7, 2011, pp. 1203-1210.

[12] T. Kaczorek, “Positive fractional continuous-time linear systems with singular pencils”, Bull. Pol. Acad. Sci. Techn., vol. 60, no. 1, 2012, pp. 9-12.

[13] T. Kaczorek, Selected Problems of Fractional Systems Theory, Springer, Berlin 2011.

[14] T. Kaczorek, “Stability of fractional positive nonlinear systems”, Archives of Control Sciences, vol. 25, no. 4, 2015, pp. 491-496.

[15] T. Kaczorek, “Global stability of positive standard and fractional nonlinear feedback systems”, Bull. Pol. Acad. Sci. Techn., vol. 68, no. 2, 2020, pp. 285-288.

[16] T. Kaczorek, “Superstabilization of positive linear electrical circuit by state-feedbacks”, Bull. Pol. Acad. Sci. Techn., vol. 65, no. 5, 2017, pp. 703-708.

[17] T. Kaczorek and K. Borawski, “Stability of Positive Nonlinear Systems”, 22nd Intern. Conf. Methods and Models in Automation and Robotics, Międzyzdroje, Poland 2017.

[18] T. Kaczorek and K. Rogowski, Fractional Linear Systems and Electrical Circuits, Springer, Cham 2015.

[19] J. Kudrewicz, “Stability of nonlinear systems with feedbacks”, Avtomatika i Telemechanika, vol. 25, no. 8, 1964 (in Russian).

[20] A. M. Lyapunov, General problem of stability movement, Gostechizdat, Moskwa, 1963 (in Russian).

[21] H. Leipholz, Stability Theory, New York Academic Press, 1970.

[22] W. Mitkowski, “Dynamical properties of Metzler systems”, Bull. Pol. Acad. Sci. Techn., vol. 56, no. 4, 2008, pp. 309-312.

[23] P. Ostalczyk, Discrete Fractional Calculus, World Scientific, River Edgle NJ 2016.

[24] I. Podlubny, Fractional Differential Equations, Academic Press, San Diego 1999.

[25] A. Ruszewski, “Stability of discrete-time fractional linear systems with delays”, Archives of Control Sciences, vol. 29, no. 3, 2019, pp. 549-567.

[26] A. Ruszewski, “Practical and asymptotic stabilities for a class of delayed fractional discrete-time linear systems”, Bull. Pol. Acad. Sci. Techn., vol. 67, no. 3, 2019, pp. 509-515.

[27] L. Sajewski, “Decentralized stabilization of descriptor fractional positive continuous-time linear systems with delays”, 22nd Intern. Conf. Methods and Models in Automation and Robotics, Międzyzdroje, Poland 2017, pp. 482-487.

[28] L. Sajewski, “Stabilization of positive descriptor fractional discrete-time linear systems with two different fractional orders by decentralized controller”, Bull. Pol. Acad. Sci. Techn., vol. 65, no. 5, 2017, pp. 709-714.